Bioinsp. Biomim. **4** (2009) 046001 (12pp) doi:10.1088/1748-3182/4/4/046001

Comparison of real and idealized cetacean flippers

P W Weber[1], M M Murray[2], L E Howle[1] and F E Fish[3]

[1] Department of Mechanical Engineering and Materials Science, Duke University, Box 90300, Durham, NC 27708, USA
[2] Department of Mechanical Engineering, United States Naval Academy, 590 Holloway Road, Annapolis, MD 21402, USA
[3] Department of Biology, West Chester University, 750 S Church Street, West Chester, PA 19383, USA

E-mail: laurens.howle@duke.edu

Received 13 February 2009
Accepted for publication 22 September 2009
Published 16 October 2009
Online at stacks.iop.org/BB/4/046001

Abstract
When a phenomenon in nature is mimicked for practical applications, it is often done so in an idealized fashion, such as representing the shape found in nature with convenient, piece-wise smooth mathematical functions. The aim of idealization is to capture the advantageous features of the natural phenomenon without having to exactly replicate it, and it is often assumed that the idealization process does in fact capture the relevant geometry. We explored the consequences of the idealization process by creating exact scale models of cetacean flippers using CT scans, creating corresponding idealized versions and then determining the hydrodynamic characteristics of the models via water tunnel testing. We found that the majority of the idealized models did not exhibit fluid dynamic properties that were drastically different from those of the real models, although multiple consequences resulting from the idealization process were evident. Drag performance was significantly improved by idealization. Overall, idealization is an excellent way to capture the relevant effects of a phenomenon found in nature, which spares the researcher from having to painstakingly create exact models, although we have found that there are situations where idealization may have unintended consequences such as one model that exhibited a decrease in lift performance.

1. Introduction

When a feature of nature is mimicked for practical applications, it is usually done so in an idealized fashion, i.e. the geometry of interest is simplified, modelled mathematically and subsequently integrated into the application. Certain elements such as the exact geometry of the item being modelled and the inherent variations among members of the same species are lost when a natural feature is idealized and modelled mathematically. It is usually assumed that the idealized design captures the relevant features of the natural feature. However, the loss of information suffered by idealizing or simplifying a design found in nature may be expected to affect performance. In this work, we explore the effect of the idealization process on the hydrodynamic performance of cetacean flippers.

One of the perhaps most well-known examples of a practical application based on a natural feature is Velcro®, which is the brand name of a hook-and-loop fastening system invented by George de Mestral based on the seeds of a burdock plant (also known as burrs) (Gebeshuber and Drack 2008). However, Velcro® does not exactly mimic the burdock seeds (burrs), rather an idealization process was performed and after much time and development the final product was produced. In the case of Velcro®, the function of the final product matched the original intent, i.e. a fastener was developed that operated similarly to natural burrs, but the idealized version differed substantially from the natural version in terms of strength, resilience, geometry and materials.

In the present work, we explore the effect of idealization on the hydrodynamic performance of cetacean flippers. Cetaceans (whales, dolphins and porpoises) use a variety of control surfaces (flukes, dorsal fins, flippers) to swim and

Report Documentation Page

Form Approved
OMB No. 0704-0188

1. REPORT DATE	2. REPORT TYPE	3. DATES COVERED
FEB 2009		**00-00-2009 to 00-00-2009**

4. TITLE AND SUBTITLE	5a. CONTRACT NUMBER
Comparison of real and idealized cetacean flippers	5b. GRANT NUMBER
	5c. PROGRAM ELEMENT NUMBER
6. AUTHOR(S)	5d. PROJECT NUMBER
	5e. TASK NUMBER
	5f. WORK UNIT NUMBER
7. PERFORMING ORGANIZATION NAME(S) AND ADDRESS(ES) **West Chester University ,Department of Biology,West Chester,PA,19383**	8. PERFORMING ORGANIZATION REPORT NUMBER
9. SPONSORING/MONITORING AGENCY NAME(S) AND ADDRESS(ES)	10. SPONSOR/MONITOR'S ACRONYM(S)
	11. SPONSOR/MONITOR'S REPORT NUMBER(S)

12. DISTRIBUTION/AVAILABILITY STATEMENT
Approved for public release; distribution unlimited

13. SUPPLEMENTARY NOTES

14. ABSTRACT

When a phenomenon in nature is mimicked for practical applications, it is often done so in an idealized fashion, such as representing the shape found in nature with convenient, piece-wise smooth mathematical functions. The aim of idealization is to capture the advantageous features of the natural phenomenon without having to exactly replicate it, and it is often assumed that the idealization process does in fact capture the relevant geometry. We explored the consequences of the idealization process by creating exact scale models of cetacean flippers using CT scans, creating corresponding idealized versions and then determining the hydrodynamic characteristics of the models via water tunnel testing. We found that the majority of the idealized models did not exhibit fluid dynamic properties that were drastically different from those of the real models, although multiple consequences resulting from the idealization process were evident. Drag performance was significantly improved by idealization. Overall, idealization is an excellent way to capture the relevant effects of a phenomenon found in nature, which spares the researcher from having to painstakingly create exact models, although we have found that there are situations where idealization may have unintended consequences such as one model that exhibited a decrease in lift performance.

15. SUBJECT TERMS

16. SECURITY CLASSIFICATION OF:			17. LIMITATION OF ABSTRACT	18. NUMBER OF PAGES	19a. NAME OF RESPONSIBLE PERSON
a. REPORT	b. ABSTRACT	c. THIS PAGE			
unclassified	**unclassified**	**unclassified**	**Same as Report (SAR)**	**12**	

manoeuvre in water. While the flukes oscillate in the vertical plane for propulsion and the dorsal fin is stationary to provide stability, the flippers are highly mobile to control a variety of underwater manoeuvres that include diving, rolling, lateral turning, braking, paddling and surfacing (Fish 2000, Fish and Battle 1995, Fish and Lauder 2002, Woodward *et al* 2006). Field observations coupled with collection and analysis of cetacean flippers have resulted in descriptions of their shapes (hereafter referred to as planforms) being catalogued.

Flipper planforms can show pronounced morphological diversification (Fish and Rohr 1999, Fish 2004). It is considered that the diversity of cetacean pectoral flipper morphologies evolved for different functions associated with each species' ecology (Howell 1930, Benke 1993). Fast-swimming oceanic dolphins (delphinids) with wing-like, highly swept-back flippers chase after rapidly moving fish and squid (Evans 1987). Flippers of delphinids may even be used to effect high-performance manoeuvres (Maresh *et al* 2004, Fish *et al* 2006). More paddle-like, broad flippers are used in low-speed manoeuvring (Benke 1993, Woodward *et al* 2006).

Flipper cross-sections are remarkably similar to those of engineered air/hydrofoils (Fish and Rohr 1999). The similarity of design indicates similar hydrodynamic performance. The streamlined profile is characterized by a rounded leading edge, slowly tapering tail and a thickness ratio (TR = maximum thickness to maximum length) of 0.14–0.33 (Webb 1975, Blake 1983). Streamlining aids in minimizing drag. The optimal TR, which provides the minimum drag for the maximum volume, is 0.22 (von Mises 1945). Streamlining reduces the magnitude of the pressure gradient over the body surface and delays separation of the boundary layer from the body. Separation occurs closer to the trailing edge resulting in a smaller wake and a reduced pressure drag. Flow visualization experiments with dolphins showed a lack of separation over the flipper surface (Rohr *et al* 1995, 1998). In addition, posterior displacement of the maximum thickness is important, because this is where transition to turbulent flow and boundary layer separation is likely to develop (Blake 1983).

The first investigation of the hydrodynamic characteristics of cetacean control surfaces examined the pressure distribution around the cross-sections of dolphin dorsal fins and flukes (Lang 1966). Fluid dynamic control by the leading-edge tubercles on the flippers of the humpback whale (*Megaptera novaeangliae*) was studied using idealized models tested in a wind tunnel (Miklosovic *et al* 2004, 2007, Johari *et al* 2007). These studies found that leading-edge tubercles delay stall when compared to versions with smooth leading edges. Miklosovic *et al* (2004, 2007) modelled the humpback whale flipper on an idealized airfoil with a cross-section based on a NACA 0020 foil. The leading edge tubercles were integrated into the idealized flipper geometry using sinusoidal functions.

The purpose of this study was to create idealized models of five different cetacean flippers and compare them to their corresponding real flippers. Such information can assist in the biomimetic design of aquatic control surfaces. The results of this study would also help to determine the effect of flipper planforms on hydrodynamic performance, as well as explore the consequences of the idealization process.

2. Materials and methods

The flippers of five species of cetaceans (fin whale, *Balaenoptera physalus*; long-finned pilot whale, *Globicephala melas*; killer whale, *Orcinus orca*; harbour porpoise, *Phocoena phocoena*; bottlenose dolphin, *Tursiops truncatus*) were obtained from deceased, stranded animals. Three-dimensional models of the flippers were created by using computed tomography (CT) scans. CT scans were obtained with a Siemens Somaton Emotion CT scanner at the Woods Hole Oceanographic Institution (Woods Hole, MA, USA) Ocean Imaging Center, a Siemens Somaton Sensation at the Mount Sinai Medical Center (New York, NY, USA), and a Toshiba Aquilion 64 at St. Joseph Hospital (Eureka, CA, USA). The details for CT scanning have been provided in Fish *et al* (2007). CT data were acquired for the entire span of each flipper (i.e. distance from anterior insertion of flipper with body to the distal tip) at 100 μm slice intervals. All images were provided as 512 $\times$ 512 matrix DICOM (Digital Imaging and Communications in Medicine format) outputs. A custom-written program in C#.NET (Microsoft Corporation, Redmond, WA, USA) was used to render the DICOM outputs into files that were readable by a computer-aided design package (SolidWorks 2008, Dassault Systèmes SolidWorks Corp., Concord, MA, USA).

Idealized flipper models were created by first fitting polynomial curves to data points obtained by considering the thickness versus height, chord versus height and height versus leading edge of the real animal flippers. The cross-section for the idealized models was then obtained by using a symmetrical NACA 00xx ('xx' means the thickness was variable) series airfoil (Abbott and von Doenhoff 1959) as the baseline, with the chord length and thickness of the NACA section obtained from the polynomial fitting (the thickness versus height and chord versus height curves). The planform shape of the idealized flipper models was generated by placing the leading edge of the idealized scaled NACA sections along the height versus leading edge fitted polynomial curve. The real and idealized flipper models were rendered using SolidWorks 2008 and were constructed using a three-dimensional rapid prototype machine (3D Systems SinterStation HiQ Series SLS System, 3D Systems, Rock Hill, SC, USA). All models were scaled due to size restrictions of the water tunnel. To minimize wall effects and tunnel blockage, the maximum allowable root to tip length of any flipper model was 20 cm, and the maximum allowable leading edge to trailing edge length was 25.4 cm. We did not consider flipper motion and our studies were limited to rigid, non-flexible flippers.

Figure 1 shows a comparison of the real and idealized planforms for the five scale models tested in this work. The planforms were classified as (1) triangular (*T. truncatus, B. physalus*), (2) swept with pointed tip (*G. melas*), (3) swept with rounded tip (*P. phocoena*), and (4) paddle shaped (*O. orca*). Table 1 shows a comparison of select geometric parameters for the real and idealized flipper models, including the scale factor. The real and idealized flipper models for each animal had mean chords, planform areas and mean thickness to chord ratios that were nearly identical, with small variances due to the curve fitting process used to create the idealized models.

Table 1. Comparison of geometry for real and idealized flipper models. The 't/c ratio' is the thickness/chord ratio. A scale less than 1 means that the flipper model is smaller than the actual animal flipper and vice versa. The real and idealized models have the same scale and length (which is defined as the root to tip distance).

Model (scale)	Type	Mean chord, $\bar{C}$ (m)	Planform area, A (cm^2)	Mean t/c ratio	Length (cm)/scale
Bottlenose dolphin (*Tursiops truncatus*)	Real	0.103	209	0.194	20/0.83
	Idealized	0.105	213	0.198	
Harbour porpoise (*Phocoena phocoena*)	Real	0.150	204	0.176	13.41/1.91
	Idealized	0.149	203	0.181	
Killer whale (*Orcinus orca*)	Real	0.110	217	0.244	20/0.33
	Idealized	0.102	207	0.234	
Fin whale (*Balaenoptera physalus*)	Real	0.064	122	0.232	20/0.32
	Idealized	0.059	120	0.239	
Long-finned pilot whale (*Globicephala melas*)	Real	0.107	115	0.159	10.82/0.43
	Idealized	0.106	116	0.160	

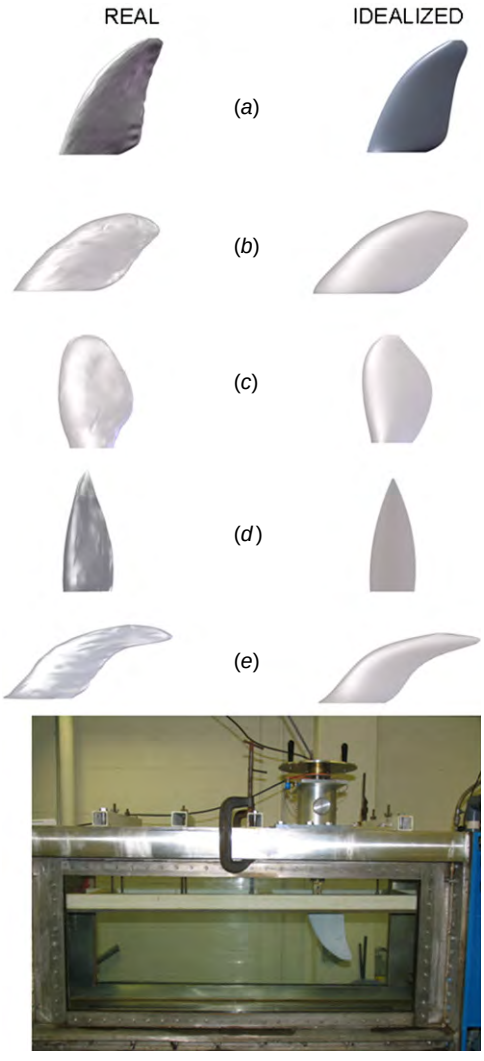

Figure 1. Real and idealized cetacean planforms tested and experimental apparatus. (*a*) Bottlenose dolphin (*Tursiops truncatus*); (*b*) harbour porpoise (*Phocoena phocoena*); (*c*) killer whale (*Orcinus orca*; (*d*) fin whale (*Balaenoptera physalus*); (*e*) long-finned pilot whale (*Globicephala melas*). The experimental apparatus with the real *T. truncatus* model mounted in the water tunnel is shown at the bottom.

Experiments were conducted in the closed-circuit water channel facility at the United States Naval Academy (USNA, Annapolis, MD, USA) Hydromechanics Laboratory. This recirculating water tunnel consists of a 0.40 m square test section that is 1.8 m long and has a velocity range of 0–6 m s^{-1}. The tunnel features flow management devices such as turning vanes in the tunnel corners and a honeycomb flow straightener in the settling chamber. The freestream turbulence intensity in the test section has been measured as ∼0.5%. Further details of the water tunnel may be found elsewhere (Schultz and Flack 2005). The flipper models were mounted in the water tunnel with a custom-designed experimental apparatus, which held the models in a known orientation and allowed for changes in the angle of attack (α). This experimental apparatus is shown in figure 1. An Advanced Mechanical Technology, Inc. Dynamometer Model UDW3-6-1000 (AMTI, Watertown, MA, USA), chosen for its capability to operate underwater, was used for measurement of flipper forces (lift and drag). LabVIEW version 8.0 (National Instruments, Austin, TX, USA) was used as the data acquisition system, and a custom-written program in C#.NET was used to post-process the data. The experimental procedure consisted of allowing the water tunnel to stabilize at the testing speed, positioning the flipper model to the desired angle of attack, collecting the data at that angle, and then manually repositioning the model to the next angle of attack. Multiple trials—a minimum of three—were conducted for each model and for each testing speed to ensure repeatability. Further details concerning model construction and experimental procedure may be found in Weber (2008).

Dynamic similarity (Shaughnessy *et al* 2005) was achieved between the actual flippers and the models by matching the Reynolds number (Re), which ensured flow similarity between the model and the animal. For this work, Re was defined as

$$\mathrm{Re} = \frac{U_{\mathrm{model}}\bar{C}_{\mathrm{model}}}{\nu_{\mathrm{model}}} = \frac{U_{\mathrm{animal}}\bar{C}_{\mathrm{animal}}}{\nu_{\mathrm{animal}}}, \qquad (1)$$

where U is the testing or animal swim velocity, $\bar{C}$ is the mean chord of the flipper model or of the actual animal flipper and ν is the kinematic viscosity of the water in which testing is conducted or in which the animal swims (which varies by

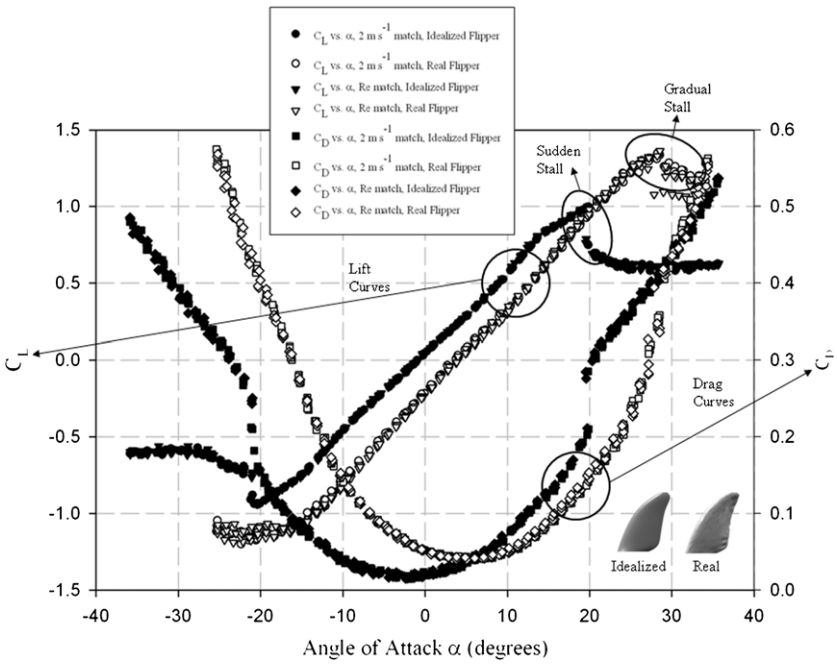

Figure 2. Experimental data for bottlenose dolphin (*Tursiops truncatus*) flipper models. The results for the idealized flipper are shown with filled symbols, while the results for the real flippers are shown with open symbols. The idealized model exhibited tip stall immediately before $C_{L,\max}$ was obtained, as evidenced by the decrease in the C_L curve slope. Also, note that the two models exhibit differing stall characteristics, with stall occurring gradually for the real model while it occurs suddenly for the idealized model.

temperature). Testing for each model was conducted at an animal swim speed of 2 m s^{-1} and a flipper Re of 250 000. This speed is the characteristic of all cetaceans, regardless of body size (Fish and Rohr 1999). Cetaceans swim at or near 2 m s^{-1} during routine swimming such as when foraging or migrating. Testing speeds were calculated by using equation (1). The swim speed value of 2 m s^{-1} was chosen for matching because it lies within the range of swim speed values observed in the wild for all animals considered in this study (Fish and Rohr 1999). The flipper Re of 250 000 was chosen for matching because it ensures that low-speed fluid dynamic phenomena such as boundary layer detachment and reattachment will not have to be considered in the analysis for those trials (i.e. at Re = 250 000 the boundary layer thickness is generally small compared to the overall length scale). The animal swim speed at the flipper Re of 250 000 was calculated for each animal to ensure that it was within the range of known swim speeds in the wild for that animal.

3. Results

Data are reported in terms of the coefficients of drag and lift,

$$C_{L,D} = \frac{2F_{L,D}}{\rho U^2 A}$$

where $F_{L,D}$ is the lift/drag force (measured by the load cell), ρ is the (incompressible) fluid density, U is the water channel testing speed and A is the planform area of the flipper model.

Finite tunnel effects were compensated for as outlined elsewhere (Barlow *et al* 1999). The maximum decrease in the lift coefficient due to finite tunnel effects for all models tested was 0.0262 (2.2%), the maximum increase in α was 1.72° and the maximum increase in the drag coefficient was 0.0429 (6.2%). Standard techniques were used to determine experimental error (Fox and McDonald 1999). Experimental error was present in many forms, including error in the load cell force readings, error in construction of the models, error in determining calibration curves and error in voltage readings. The method that we used to determine overall experimental error took these and other factors into account, and also determined the overall relative effects of these errors (for example, the error in determining the water tunnel speed depended on both the error in the Pitot tube calibration curve and the error in the voltage reading). The maximum uncertainty in the water tunnel speed was ±7.2%, the maximum uncertainty in the Reynolds number was ±7.7% and the maximum uncertainty in lift and drag coefficient measurements was ±15.1%. The experimental error for many of the models tested was actually less than these maximum errors; for example, when water tunnel speed was increased, the relative uncertainty in the tunnel speed was reduced, which in turn meant that the error in the lift and drag coefficient measurements was reduced.

Figures 2–6 present the results of the experimental studies, broken down by individual animal (figure 2: bottlenose dolphin (*T. truncatus*), figure 3: harbour porpoise (*P. phocoena*), figure 4: killer whale (*O. orca*), figure 5: fin whale (*B. physalus*), figure 6: long-finned pilot whale (*G. melas*)). Each figure shows plots of C_L and C_D versus α for both the real flipper model (open symbols) and the idealized flipper model (filled symbols) over a range of α. The data for both trials (swim speed match and Re match) are presented on the same graph. These figures qualitatively and quantitatively show the differences in performance between the real and idealized

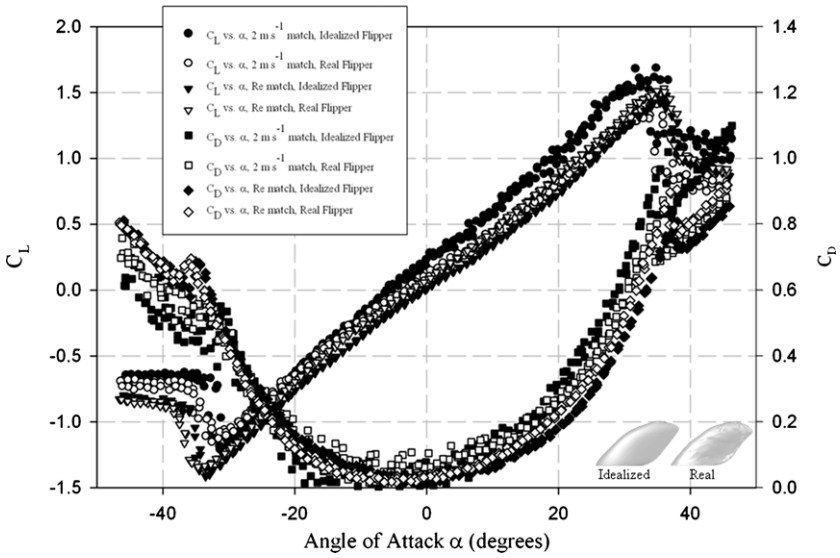

Figure 3. Experimental data for harbour porpoise (*Phocoena phocoena*) flipper models. The results for the idealized flipper are shown with filled symbols, while the results for the real flippers are shown with open symbols. Note the nonlinear nature of the lift curves. The spread in the data for the C_D curves is due to the load cell having difficultly resolving the small forces at the relatively slow flow speed.

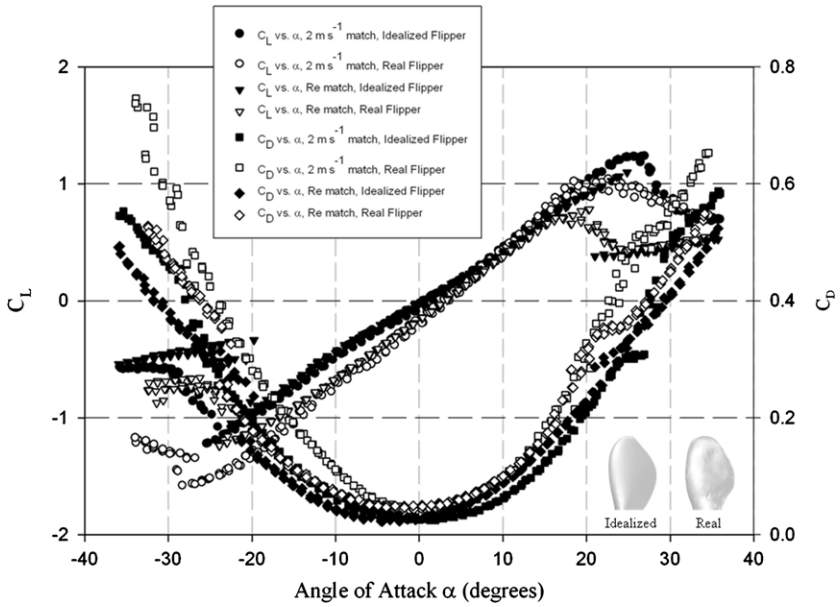

Figure 4. Experimental data for killer whale *Orcinus orca* flipper models. The results for the idealized flipper are shown with filled symbols, while the results for the real flippers are shown with open symbols. The stall characteristics differ for the Re match trial, with the idealized model losing lift suddenly at stall while the real model stalls gradually. This disparity in stall characteristics is not present for the 2 m s^{-1} match trial due to the higher Re of 674 000.

models. Tables 2 and 3 present hydrodynamic parameters of interest for the Re match trials (table 2) and the 2 m s^{-1} match trials (table 3). These parameters include the maximum lift coefficient ($C_{L,\max}$), the minimum drag coefficient ($C_{D,\min}$) and the slope(s) of the C_L versus α curve. Table 2 additionally presents what the animal swim speed would be at the flipper Re of 250 000 that was tested, and table 3 additionally presents the value of the animal flipper Re at the animal swim speed of 2 m s^{-1} that was tested. Table 4 presents the maximum hydrodynamic efficiency $(C_L/C_D)_{\max}$ (Anderson 2001) for all models tested by trial.

As seen in tables 2 and 3, the idealized flipper models had a lower $C_{D,\min}$ than the real flipper models for all trials. The least difference was for the *B. physalus Re* match trial, where the $C_{D,\min}$ for the real flipper model was 23% greater than that for the idealized model, and the greatest difference was for the *P. phocoena* 2 m s^{-1} trial, where the $C_{D,\min}$ for the real model was 176% greater than that for the idealized model. On average, $C_{D,\min}$ was 96% greater for the real models than for the idealized models. Additionally, figures 2–6 show that when experimental trials are compared (2 m s^{-1} match or Re match), the C_D versus α for the idealized flippers was lower

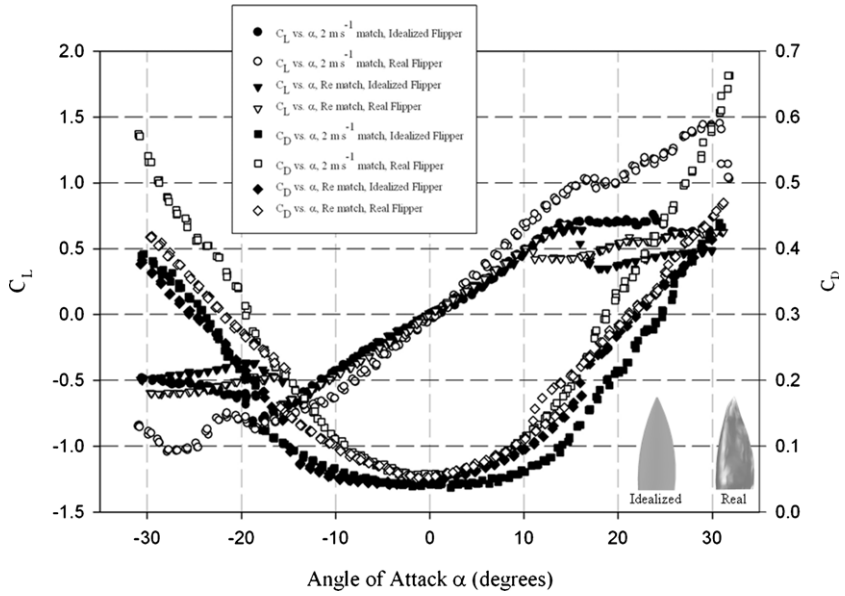

Figure 5. Experimental data for fin whale (*Balaenoptera physalus*) flipper models. The results for the idealized flipper are shown with filled symbols while the results for the real flippers are shown with open symbols. The idealized model exhibits a nonlinear C_L curve, while the real model does not (see explanation in the text). Additionally, the stall characteristics differ for the Re match trial, with the real model experiencing a sudden loss of lift, while the idealized model stalls gradually. The stall characteristics do not differ for the 2 m s^{-1} trial where the Re is 398 000.

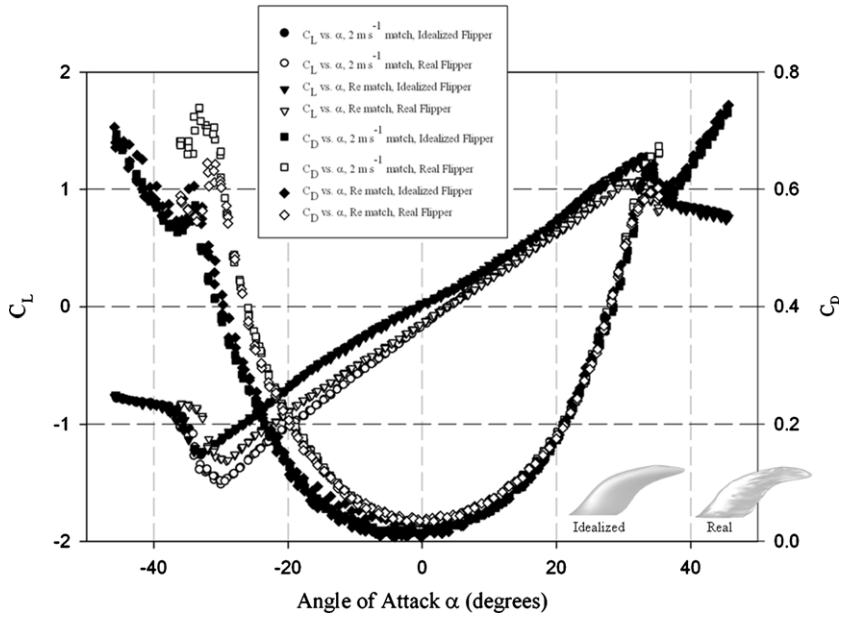

Figure 6. Experimental data for long-finned pilot whale *Globicephala melas* flipper models. Note the nonlinear nature of the lift curves. The results for the idealized flipper are shown with filled symbols, while the results for the real flippers are shown with open symbols. There is no meaningful difference in stall characteristics between the two models.

over the non-stall region and over most of the stall region as well when compared to the real flippers.

When the C_L versus α curves for the real and idealized flippers are compared, a clear relation, such as that found for the C_D versus α curves, is not found to exist. For *T. truncatus* and *B. physalus*, the real flipper models produced a higher $C_{L,\max}$ for both trials. The $C_{L,\max}$ for the real *T. truncatus* model was 36% higher than that for the idealized model for the Re match trial and 35% higher for the 2 m s^{-1} match trial, and the $C_{L,\max}$ for the real *B. physalus* model was 6% higher than that for the idealized model for the Re match trial and 105% greater for the 2 m s^{-1} match trial. In contrast, for *O. orca* and *G. melas*, the idealized flipper models produced a higher $C_{L,\max}$ for both trials. The $C_{L,\max}$ for the idealized *O. orca* model was 40% higher than that for the real model for the Re match trial and 19% higher for the 2 m s^{-1} match trial, and the $C_{L,\max}$ for the idealized *G. melas* model was 19% higher than that for the real model for the Re match trial

Table 2. Select hydrodynamic performance parameters for the real and idealized cetacean flipper models tested, Reynolds number of 250 000 match trials.

Model	Type	$C_{L,\max}$	$C_{D,\min}$	Animal swim speed at flipper Re of 250,000 (m s^{-1})	Linear portion(s) C_L curve slope (1/deg)
Bottlenose dolphin (*Turiops truncatus*)	Real	1.362	0.0397	2.14	0.0589
	Idealized	1.000	0.0151	2.14	0.0522
Harbour porpoise (*Phocoena phocoena*)	Real	1.531	0.0162	4.16	0.0493 ($C_{L,\min}$ to −12), 0.0351 (−12 to 8), 0.0431 (8 to $C_{L,\max}$)
	Idealized	1.478	0.0129	4.16	0.0444 ($C_{L,\min}$ to −4), 0.0312 (−4 to 8), 0.0443 (8 to $C_{L,\max}$)
Killer whale (*Orcinus orca*)	Real	0.7839	0.0441	0.742	0.0505
	Idealized	1.099	0.0228	0.742	0.0449
Fin whale (*Balaenoptera physalus*)	Real	0.6894	0.0510	1.26	0.0469
	Idealized	0.6498	0.0415	1.26	0.0560 ($C_{L,\min}$ to −6), 0.0392 (−6 to 7), 0.0617 (7 to 12)
Long-finned pilot whale (*Globicephala melas*)	Real	1.065	0.0331	1.31	0.0500 ($C_{L,\min}$ to −26), 0.0375 (−26 to 17), 0.0417 (17 to $C_{L,\max}$)
	Idealized	1.263	0.0176	1.31	0.0424 ($C_{L,\min}$ to −9), 0.0302 (−9 to 9), 0.0415 (9 to $C_{L,\max}$)

Table 3. Select hydrodynamic performance parameters for the real and idealized cetacean flipper models tested, 2 m s^{-1} swim speed match trials.

Model	Type	$C_{L,\max}$	$C_{D,\min}$	Animal flipper Re at swim speed	Linear portion(s) C_L curve slope (1/deg)
Bottlenose dolphin (*Turiops truncatus*)	Real	1.345	0.0397	234 000	0.0574
	Idealized	0.9972	0.0148	234 000	0.0517
Harbour porpoise (*Phocoena phocoena*)	Real	1.410	0.0456	120 000	0.0417 ($C_{L,\min}$ to −6), 0.0313 (−6 to 8), 0.0407 (8 to $C_{L,\max}$)
	Idealized	1.686	0.0165	120 000	0.0480 ($C_{L,\min}$ to −6), 0.0365 (−6 to 6), 0.0461 (6 to $C_{L,\max}$)
Killer whale (*Orcinus orca*)	Real	1.040	0.0356	674 000	0.0575
	Idealized	1.241	0.0248	674 000	0.0489
Fin whale (*Balaenoptera physalus*)	Real	1.452	0.0545	398 000	0.0649
	Idealized	0.7072	0.0372	398 000	0.0508 ($C_{L,\min}$ to −7), 0.0397 (−7 to 4), 0.0530 (4 to 14)
Long-finned pilot whale (*Globicephala melas*)	Real	1.217	0.0305	381 000	0.0479 ($C_{L,\min}$ to −25), 0.0376 (−25 to 25), 0.0430 (25 to $C_{L,\max}$)
	Idealized	1.277	0.0129	381 000	0.0431 ($C_{L,\min}$ to −8), 0.0290 (−8 to 8), 0.0433 (8 to $C_{L,\max}$)

and 5% greater for the 2 m s^{-1} match trial. The *P. phocoena* models were unique in that the real flipper model produced a 4% higher $C_{L,\max}$ than the idealized flipper model for the Re match trial, while the idealized flipper model produced a 20% higher $C_{L,\max}$ than the real flipper model for the 2 m s^{-1} match trial.

The C_L versus α curves for *P. phocoena* and *G. melas* were observed to be nonlinear in the non-stall region for both the real and idealized models (figures 3, 6). Both of these flippers have planforms that are similar to those of modern swept wings. Additionally, the C_L versus α curves for *B. physalus* were found to be nonlinear for the idealized model but not for the real model (figure 5). All other C_L versus α curves exhibited linear behaviour in the non-stall region.

The C_L curve slopes were found to be comparatively closer in value between the real and idealized models than the

Table 4. Maximum hydrodynamic efficiency $(C_L/C_D)_{\max}$ for the real and idealized cetacean models tested.

Model	Type	$(C_L/C_D)_{\max}$ (Re match trial)	$(C_L/C_D)_{\max}$ (2 m s^{-1} match trial)
Bottlenose dolphin (*Tursiops truncatus*)	Real	7.90	7.57
	Idealized	8.70	8.79
Harbour porpoise (*Phocoena phocoena*)	Real	5.85	6.69
	Idealized	6.21	8.88
Killer whale (*Orcinus orca*)	Real	4.00	4.63
	Idealized	4.87	7.53
Fin whale (*Balaenoptera physalus*)	Real	4.57	6.18
	Idealized	5.20	8.23
Long-finned pilot whale (*Globicephala melas*)	Real	3.88	4.18
	Idealized	8.68	6.69

values of $C_{L,\max}$. The maximum difference in the C_L curve slope between the real and idealized models was found to be 38.8% for the *B. physalus* 2 m s^{-1} trial, while the minimum difference was found to be 0.7% for the *G. melas* 2 m s^{-1} trial. The average difference across all models and trials was found to be 14.9%.

All of the C_L versus α curves exhibited stall characteristics (figures 2–6), where the C_L curve increases to a maximum value ($C_{L,\max}$) and then subsequently decreases due to flow separation causing loss of lift. The idealization process was found to change the nature of stall for three of the five models tested, although not always for both the 2 m s^{-1} speed match trial and Re match trial (only four of the ten overall trials showed varying stall characteristics between the real and idealized models).

Table 4 shows that the maximum hydrodynamic efficiency for the idealized models is always greater than that for the real models. Hydrodynamic efficiency is defined as $(C_L/C_D)_{\max}$ and gives an indication of the drag force that is produced for a certain value of lift force (Anderson 2001). An efficiency greater than 1 means that more lift force is being generated than drag force (which is usually desired) and vice versa. The maximum efficiency occurs at different values of α for different flippers and does not necessarily occur at the same α as the $C_{L,\max}$ and/or the $C_{D,\min}$. The greatest gain in $(C_L/C_D)_{\max}$ due to the idealization process was 124% (*G. melas* Re match trial), the least gain in $(C_L/C_D)_{\max}$ was 6% (*P. phocoena* Re match trial) and the average gain in $(C_L/C_D)_{\max}$ was 38%.

4. Discussion

The idealization process had a significant effect on both $C_{D,\min}$ and the overall drag characteristics of the flipper models. The principal explanation for the differences in drag is the fact that the idealized models had cross-sections that were more streamlined. Modern engineered airfoil sections (such as the NACA series of airfoil sections that were used here) are specifically designed to minimize drag, so the results from the experiment are not surprising. An additional explanation for the differences in drag characteristics seen here is the fact that the idealized flipper models had surfaces that were much smoother in comparison to the real models. Surface imperfections increase drag. The boundary layer is affected by bumps and other surface irregularities, and the boundary layer often changes character (i.e. transitions from laminar to turbulent) when it encounters a surface irregularity (Hoerner 1992). In addition, surface imperfections (particularly protrusions on the surface) produce local additional drag and this local drag scales with the size of the protrusion (Hoerner 1992). The additional drag caused by surface irregularities will vary depending upon individual variation of the flipper. The fact that C_D was always less for the idealized models than for the real models also explains why the efficiency for the idealized models was always greater than that for the real models. Since efficiency is defined as $(C_L/C_D)_{\max}$, it naturally follows that when C_D is reduced then efficiency is automatically raised with all other factors being equal.

When the C_L versus α curves for the real and idealized flipper models were compared, no clear trend was found (i.e. idealized flipper models did not consistently have a higher $C_{L,\max}$ than real flipper models). One possible explanation for this lack of a clear trend is the camber of the flippers. For any airfoil, a mean line may be drawn from the leading edge to the trailing edge that is equidistant from the upper surface and the lower surface. If this mean line is curved, then the airfoil is said to be cambered (see Shaughnessy *et al* 2005, Fox and McDonald 1999, or Abbott and von Doenhoff 1959 for an exact engineering definition). The camber of the flippers is an important consideration, because $C_{L,\max}$ increases with increasing camber (Abbott and von Doenhoff 1959). All of the idealized flippers were constructed from symmetric NACA sections, so they were all uncambered and therefore did not experience any increase in $C_{L,\max}$ due to camber. However, the real flipper models all had some camber due to their natural non-symmetric geometry. Therefore, the superior performance of the real *T. truncatus*, *P. phocoena* and *B. physalus* flipper models over the idealized models could be due to the gain in $C_{L,\max}$ from their natural camber. Furthermore, the fact that the idealized *P. phocoena* model outperformed the real model for the 2 m s^{-1} match trial (but not for the Re match trial) can be explained by the fact that the effect of camber increasing $C_{L,\max}$ is more pronounced for higher Re (Abbott and von Doenhoff 1959). For the *P. phocoena* 2 m s^{-1} match trial, the Re was only 120 000, so the gain in $C_{L,\max}$ that the real flipper experienced due to camber may not have been sufficient to outperform the idealized model (and it follows that the gain was sufficient at Re = 250 000). Additionally, at this (relatively) low Re of 120 000 for the 2 m s^{-1} match trial, boundary layer effects are more pronounced (White 2006), which may cause phenomena such as unsteadiness and flow detachment/reattachment. One observation for *P. phocoena* which may be caused by low Re effects is that the α of zero lift (i.e. the α at which $C_L = 0$) was negative for the 2 m s^{-1} match trial while it was approximately zero for the Re match trial. This difference in the angle of zero lift between trials was not seen for any other flipper. Since the flipper geometry did not change between trials, changes in fluid dynamic phenomena related to Re effects are the likely culprit.

The nonlinear nature of the lift curves for the real and idealized *P. phocoena* and *G. melas* models and the idealized *B. physalus* model is caused by two different lift mechanisms acting in the non-stall region. For low α, potential lift is the dominant lift mechanism. For higher α, the lift-generation mechanism transitions to vortex-dominated lift, characterized by strong vortices that form on the surface of the flipper (i.e. move from the flipper tip towards the root) and an increase in the C_L curve slope (Hoerner and Borst 1985). These vortices generate low pressures which contribute to the lift and are a well-known occurrence for modern delta wings (Houghton and Carpenter 2003). The values of the C_L curve slope for both the potential flow region (lower slope) and the vortex-dominated flow regions (higher slope) are shown in tables 1 and 2.

The data presented here indicate that the idealization process can change the nature of the C_L curve, but does not necessarily do so. For *P. phocoena* and *G. melas*, the planform is the dominant mechanism that causes the nonlinear nature of the lift curve, as evidenced by the fact that the nonlinearity was still captured by the idealized model. For the *B. physalus* models, it appears that the idealization process sufficiently changed the model to cause the nonlinear C_L curve, that is, the real flipper model generates potential lift while the idealized model generates vortex-dominated lift. Figure 1 shows that the idealization process for *B. physalus* produced a geometry with smooth leading and trailing edges that end in a sharp point at the tip. In contrast, the real model had leading and trailing edges that were less smooth, and the point at the tip was not as sharp. Additionally, there is a difference in the cross-sections of the real and idealized models. The cross-sections for the idealized models were perfectly streamlined (via a NACA profile). The cross-sections of the real models were generally streamlined (i.e. they had a rounded leading edge tapering down to a thin trailing edge), but unlike engineered foils they were generally not sharp at the trailing edge and the upper and lower surfaces were irregular as opposed to smooth.

To visualize the flow field around the flipper models and to explore the differences in lift characteristics between the real and idealized *B. physalus* models, the computational fluid dynamics (CFD) code COSMOS FloWorks (an add-in to SolidWorks 2008, Dassault Systèmes SolidWorks Corp., Concord, MA, USA) was used to calculate the fluid pathlines around both the real and idealized models for *P. phocoena* and *B. physalus*. A *pathline* is the trajectory that a selected fluid particle follows in a flow field (Shaughnessy *et al* 2005). FloWorks uses the finite volume method to solve the Reynolds-averaged Navier–Stokes (RANS) equations, implementing the $k-\varepsilon$ turbulence model. Figure 7 shows the results of the CFD simulations for *P. phocoena* ($U = 1.68$ m s^{-1}, $\alpha = 4.5^\circ$ and 10° and Re $= 250\,000$) and *B. physalus* ($U = 3.93$ m s^{-1}, $\alpha = 14^\circ$ and Re $= 250\,000$). The results of the CFD simulations were checked against the experimental values to ensure that the results were accurate to within experimental and computational errors (an exemplary plot is shown in the centre of figure 7). The comparison shows that the CFD predictions are excellent in the non-stall region. However, when stall is encountered, the lift and drag are both under-predicted due to the complex flow field which is characterized by regions of flow separation, which is difficult to model numerically. Despite these under-predictions, it is seen that the CFD still qualitatively predicts the correct shape of the lift and drag curves.

For both models (*P. phocoena* and *B. physalus*), it was found that the wake for the idealized flipper model was less disturbed than that of the real flipper model. This was most likely due to the streamlining of the idealized flipper model cross-sections. Additionally, the flow over the idealized flipper model surfaces was seen to be smoother than that of the real flipper models. This was due to the smoothness of the idealized flipper surface, as the fluid did not have to flow around or through protuberances on the surface as it did with the real model. Differences in the tip vortices were also observed for both models (figure 7).

The qualitative difference in the flow fields between the potential lift regime and the vortex-dominated lift regime for *P. phocoena* is evident from figure 7. For the potential lift regime (denoted as A and B in figure 7), the flow around the flippers is seen to be smooth and the pathlines are generally parallel in the wake, with the exception of the tip vortex. However, when α is increased to the vortex-dominated lift regime (denoted as C in figure 7), a strong vortex forms over the planform of the flipper, and fluid over most of the leading edge is entrained into this vortex. This effect is not as pronounced as it is for an engineered delta wing because the sharpness of the leading edge is intimately related to the strength of the vortex, and cetacean flippers have rounded leading edges. As the leading edge becomes sharper, the leading edge suction is more prominent causing greater acceleration, which results in a stronger vortex and more suction force (Katz and Plotkin 2001).

Using these CFD simulations, it is seen that the reason that the idealized *B. physalus* model C_L curve is nonlinear while the real model curve is linear may be explained by two factors. The first factor is the artificially sharp tip of the idealized model when compared to the real model. The shape of the flipper tip affects the location of the tip vortex and the value of $C_{L,\max}$ (Hoerner and Borst 1985), and it appears that the sharp tip of the idealized flipper model in combination with the local sweep of the flipper at the tip caused the tip vortex to move towards the root at high α and produce the vortex-dominated lift. This may be seen in the flow visualization in figure 7, where the real model (denoted as D in figure 7) exhibits a strong trailing vortex that is localized at the tip (with a weaker vortex forming further up towards the root), whereas the idealized model (denoted as E in figure 7) exhibits a trailing vortex that forms at a distance of approximately $3/4$ of the distance of the flipper length from the root with no tip vortex. The second factor is that the streamlined cross-section of the idealized flipper provides less resistance to the movement of the tip vortex inward. The protuberances on the surface of the real flipper model could act similar to a vortex fence, which prevents the flow from moving spanwise across the flipper (Hoerner and Borst 1985). Figure 7 again shows that for the idealized *B. physalus* model, flow in the vicinity of the tip is still relatively smooth, one primary vortex forms at the $3/4$ distance from the root, and the flow around the tip

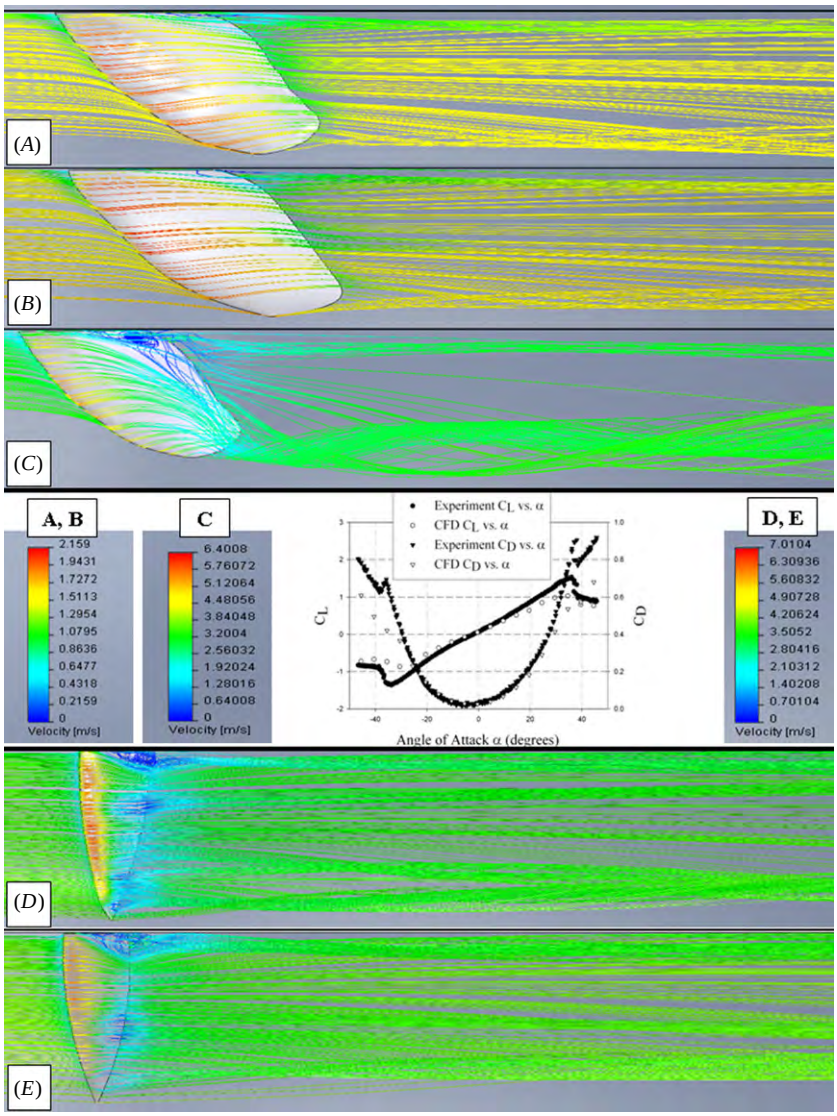

Figure 7. Numerically calculated pathlines for (*A*) real harbour porpoise (*Phocoena phocoena*), $U = 1.68$ m s^{-1}, $\alpha = 4.5^\circ$, Re = 250 000; (*B*) idealized *P. phocoena*, $U = 1.68$ m s^{-1}, $\alpha = 4.5^\circ$, Re = 250 000; (*C*) real *P. phocoena*, $U = 1.68$ m s^{-1}, $\alpha = 20^\circ$, Re = 250 000; (*D*) real fin whale (*Balaenoptera physalus*), $U = 3.93$ m s^{-1}, $\alpha = 10^\circ$, Re = 250 000; and (*E*) idealized *B. physalus*, $U = 3.93$ m s^{-1}, $\alpha = 10^\circ$, Re = 250 000. The graph in the centre compares the experimental and CFD results for the real *P. phocoena* flipper model.

moves towards the root and is entrained into this strong vortex, which produces the vortex-dominated lift. However, for the real model, two vortices form, one strong vortex off of the tip and then a secondary weaker vortex at 3/4 of the distance from the root. This weaker vortex for the real model is entrained into the strong tip vortex farther downstream. Tip stall is seen to develop for the real model, which also contributes to the tip vortex not being able to move towards the root and produce the vortex-dominated lift. So, our conclusion is that the geometry of the real flipper along with surface effects prevents the tip vortex from moving towards the root and therefore keeps the lift in the potential regime.

The overall reason for the difference in stall characteristics between some real and idealized models is that wings are known to display different stall characteristics at different values of Re, most notably at low values (Hoerner and Borst 1985). The models for *T. truncatus* were the most disparate overall (figure 2). For the *O. orca* flipper models at Re = 250 000, the real flipper model exhibited a gradual loss of lift at stall, while the idealized model exhibited a sudden loss of lift at stall (figure 4). When the Re was increased to 674 000, both models were characterized by a gradual loss of lift at stall. For the *B. physalus* flipper models at Re = 250 000, the real flipper model exhibited a sudden drop in lift at stall, while the idealized model exhibited a gradual loss of lift at stall (figure 5). However, when the Re was increased to 398 000 both models exhibited gradual stall. These data appear to indicate that there is a unique value of Re for each flipper above which creating an idealized model will not change the stall characteristics, although further experimentation must be performed to confirm this hypothesis and determine exact values.

The C_L versus α curves provide a general sense of the camber for the real flippers and the degree of construction

error for the idealized flippers. The angle of zero lift $\alpha_{L=0}$ (defined as the value of α where the C_L versus α curve is zero) is largely determined by the camber (Abbott and von Doenhoff 1959). A flipper that has a negative value of $\alpha_{L=0}$ (and therefore produces a positive value of lift at $\alpha = 0^\circ$) is said to be positively cambered and vice versa. Theoretically, an uncambered flipper (such as all of the idealized flippers) should have an $\alpha_{L=0}$ of zero. For the real flippers, *T. truncatus*, *O. orca* and *G. melas* were found to be negatively cambered, *P. phocoena* was found to be positively cambered and *B. physalus* had essentially no camber. For the idealized flippers, *G. melas*, *O. orca* and *B. physalus* appeared to have minimal construction error as their values of $\alpha_{L=0}$ were zero to within experimental error. The idealized *T. truncatus* model appeared to have a slight bias in the positively cambered direction during construction since $\alpha_{L=0} \approx -1^\circ$. At first glance, the idealized model for *P. phocoena* appeared to have severe bias in the positively cambered direction since, for this flipper, $\alpha_{L=0} \approx -6^\circ$for the 2 m s^{-1} speed match trial. However, low Re effects (Re = 120 000 in this case) were the most likely reason for the bias since $\alpha_{L=0}$ was essentially zero when the Re was increased to 250 000.

Construction error in the models as well as experimental error was evident in the fact that the C_L and C_D versus α curves for the idealized flipper models were not perfectly symmetric (figures 2–6). If construction and experimental error do not exist, the C_L versus α curve for an idealized flipper model based off of a symmetrical NACA section should be an odd function (i.e. symmetric with respect to a 180° rotation about the origin) that intersects the α-axis at a value of 0°. Similarly, the C_D versus α curve should be an even function (i.e. symmetric with respect to the C_D-axis) with a minimum value of $C_{D,\min}$ occurring at $\alpha = 0$. There are multiple possible explanations for the fact that the idealized model curves were not perfectly symmetric. The first possibility is error in the construction of the models. The three-dimensional rapid prototype machine does not create absolutely perfect models due to a variety of factors such as the material containing impurities, calibration of the machine and thermal deformation of the model during the manufacturing process. These imperfections are not evident by sight inspection (otherwise the model would have been discarded and rebuilt), but can account for the small disparities in the curves. Another possibility is experimental error. For example, the measurement of α has experimental error associated with it, so a model may have $C_L = 0$ or $C_{D,\min}$ occurring at $\alpha = 0$, but the experimental angle reading will not indicate so. Another source of experimental error is the fact that the water tunnel does not create perfectly uniform flow. A final possible explanation for the idealized curves not being perfectly symmetric is miniscule variations in the surface roughness of the idealized flippers. As previously mentioned, the surfaces of the idealized models were much smoother and more uniform than those of the real models, but microscopic imperfections still exist on the surfaces of the idealized models. These imperfections could cause the curves to not be perfectly symmetric, especially in the near-stall and post-stall regions where boundary layer effects are very important.

Overall, the majority of the idealized models of cetacean flippers did not exhibit fluid dynamic properties that were drastically different from those of the models of the real flippers, although multiple consequences resulting from the idealization process were evident. For example, $C_{D,\min}$ of the idealized models was less than the corresponding $C_{D,\min}$ of the real models for all trials, which indicates that idealization can have a significant advantage if one is attempting to minimize drag and can result in performance which is better than that which is found in nature. $C_{L,\max}$ for the real and corresponding idealized models was different for all trials, and was improved in some cases by the idealization process and worsened in others. The hydrodynamic efficiency $(C_L/C_D)_{\max}$ was always greater for the idealized models over their corresponding real model counterparts, again showing an instance where idealization results in performance that is more advantageous than that which is found in nature. Stall characteristics were sometimes varied by the idealization process, usually at lower Re. One model, *B. physalus*, demonstrated the unintended consequence of its C_L versus α curve being changed from linear to nonlinear due to the idealization process. The principal causes of the variations in hydrodynamic performance were differences in the smoothness of the flipper surfaces and the streamlining of the idealized flipper cross-sections using a NACA airfoil profile.

In conclusion, this work represents multiple findings that will be of interest to future researchers that create idealized models of phenomena found in nature. The first and most important is that idealized models of phenomena found in nature reasonably represent the performance of the real models on which they are based, as has been assumed in the past but has been verified here. Of course, there are some differences (such as the drag characteristics), but these are usually known or may be deduced by the researcher. However, we have also shown that it is necessary to be reasonably cautious with the results, as idealization can sometimes have unintended consequences. The second (which is a consequence of the first) is that when mimicking a phenomenon found in nature, it is not necessary to go through the painstaking process of trying to exactly reproduce the desired attribute through collection and analysis of biological specimens. In fact, for the cetacean flippers we explored in this work, it would only be necessary to obtain photographs of the geometry of interest to create an idealized model. This is especially useful when attempting to study animals for which biological specimens are difficult to obtain (such as an endangered animal) or impossible to obtain (such as an extinct animal). As long as the dimensions of the geometry are known (i.e. photograph) or may be extrapolated (i.e. fossil record), an idealized model may be created and the experimental data may be used with confidence. Our final finding is that for idealized models of cetacean flippers, we have presented quantitative bounds on the difference between performance characteristics for real and idealized models which may be used in future research. For example, we found that the maximum difference in the C_L curve slope between the real and idealized models tested was 38.8% and the average was 14.9%. So, if an idealized

model with a geometry that is reasonably similar to the ones presented in this work is tested in the future, the performance of the real model may be bounded by these values of maximum difference. Overall, idealization is and will continue to be an important method by which to learn from nature.

Acknowledgments

This work was supported by the National Science Foundation (FEF: principal investigator) and the technical support staff of the United States Naval Academy. PWW was supported by the National Defense Science and Engineering Graduate (NDSEG) Fellowship. The authors additionally would like to thank the New Bolton Center of the University of Pennsylvania Veterinary School, the New Jersey Marine Mammal Stranding Center, the Woods Hole Oceanographic Institution, St Joseph Hospital, the Humboldt State University Vertebrate Museum, and specially J Arruda, S Cramer, P Habecker, D Ketten, C Ginter, J Parson, J Reidenberg, R Schoelkopf, J Jacobsen, S Wallis and B Schuelkens for contributions to this work.

References

Abbott I H and von Doenhoff A E 1959 *Theory of Wing Sections* (New York: Dover)

Anderson J D 2001 *Fundamentals of Aerodynamics* 3rd edn (New York: McGraw-Hill)

Barlow J B, Rae W H and Pope A 1999 *Low-Speed Wind Tunnel Testing* 3rd edn (New York: Wiley)

Benke H 1993 Investigations on the osteology and the functional morphology of the flipper of whales and dolphins (*Cetacea*) *Investig. Cetacea* **24** 9–252

Blake R W 1983 *Fish Locomotion* (Cambridge: Cambridge University Press)

Evans P G H 1987 *The Natural History of Whales & Dolphins* (New York: Facts on File)

Fish F E 2000 Biomechanics and energetics in aquatic and semiaquatic mammals: platypus to whale *Physiol. Biochem. Zool.* **73** 683–98

Fish F E 2004 Structure and mechanics of nonpiscine control surfaces *IEEE J. Ocean. Eng.* **29** 605–21

Fish F E and Battle J M 1995 Hydrodynamic design of the humpback whale flipper *J. Morphol.* **225** 51–60

Fish F E, Beneski J T and Ketten D R 2007 Examination of the three-dimensional geometry of cetacean flukes using computed tomography scans: hydrodynamic implications *Anat. Rec.* **290** 614–23

Fish F E and Lauder G V 2002 Passive and active flow control by swimming fishes and mammals *Ann. Rev. Fluid Mech.* **38** 193–224

Fish F E, Nicastro A J and Weihs D 2006 Dynamics of the aerial maneuvers of spinner dolphins *J. Exp. Biol.* **209** 590–8

Fish F E and Rohr J 1999 Review of dolphin hydrodynamics and swimming performance *Technical Report No* 1801 (San Diego, CA: SPAWARS System Center)

Fox R W and McDonald A T 1999 *Introduction to Fluid Mechanics* 5th edn (New York: Wiley)

Gebeshuber I C and Drack M 2008 An attempt to reveal synergies between biology and mechanical engineering *Proc. Inst. Mech. Eng.* C **222** 1281–7

Hoerner S F 1992 *Fluid-Dynamic Drag* (Bakersfield, CA: Author)

Hoerner S F and Borst H V 1985 *Fluid-Dynamic Lift* 2nd edn (Bakersfield, CA: Author)

Houghton E L and Carpenter P W 2003 *Aerodynamics for Engineering Students* 5th edn (New York: Elsevier Butterworth-Heinemann)

Howell A B 1930 *Aquatic Animals* (Springfield, IL: Charles C Thomas)

Johari H, Henoch C, Custodio D and Levshin A 2007 Effects of leading edge protuberances on airfoil performance *AIAA J.* **45** 2634–42

Katz J and Plotkin A 2001 *Low-Speed Aerodynamics* 2nd edn (Cambridge, UK: Cambridge University Press)

Lang T G 1966 Hydrodynamic analysis of dolphin fin profiles *Nature* **209** 1110–1

Maresh J L, Fish F E, Nowacek D P, Nowacek S M and Wells R S 2004 High performance turning capabilities during foraging by bottlenose dolphins *Mar. Mamm. Sci.* **20** 498–509

Miklosovic D S, Murray M M and Howle L E 2007 Experimental evaluation of sinusoidal leading edges *J. Aircraft* **44** 1404–7

Miklosovic D S, Murray M M, Howle L E and Fish F E 2004 Leading-edge tubercles delay stall on humpback whale (*Megaptera novaeangliae*) flippers *Phys. Fluids* **16** L39-42

Rohr J, Latz M I, Fallon S, Nauen J C and Hendricks E 1998 Experimental approaches towards interpreting dolphin-stimulated bioluminescence *J. Exp. Biol.* **201** 1447–60

Rohr J, Latz M I, Hendricks E and Nauen J C 1995 A novel flow visualization technique using bioluminescent marine plankton—part II: field studies *IEEE J. Ocean. Eng.* **20** 147–9

Schultz M P and Flack K A 2005 Outer layer similarity in fully rough turbulent boundary layers *Exp. Fluids* **38** 328–40

Shaughnessy E J, Katz I M and Schaffer J P 2005 *Introduction to Fluid Mechanics* (New York: Oxford University Press)

von Mises R 1945 *Theory of Flight* (New York: Dover)

Webb P W 1975 Hydrodynamics and energetics of fish propulsion *Bull. Fish. Res. Bd. Can.* **190** 1–159

Weber P W 2008 Hydrodynamic characteristics of marine animal control surfaces *MS Thesis* Department of Mechanical Engineering, Duke University, Durham, NC, USA

White F M 2006 *Viscous Fluid Flow* 3rd edn (Boston, MA: McGraw-Hill)

Woodward B L, Winn J P and Fish F E 2006 Morphological specializations of baleen whales associated with hydrodynamic performance and ecological niche *J. Morphol.* **267** 1284–94